RSC Advances

PAPER

View Article Online
View Journal | View Issue

Cite this: RSC Adv., 2015, 5, 86237

Effect of degree of reduction on the anode performance of reduced graphene oxide in Li-ion batteries†

Sujin Kim,[a] Gyutae Park,[a] Palanichamy Sennu,[b] Seungjun Lee,[a] Kwangrok Choi,[a] Junghoon Oh,[a] Yun-Sung Lee[b] and Sungjin Park*[a]

Received 15th July 2015
Accepted 6th October 2015

DOI: 10.1039/c5ra13890f

www.rsc.org/advances

Graphene-based materials are considered to be promising anodes for achieving high energy and power densities in Li-ion batteries (LIBs). Despite intensive research on reduced graphene oxide (rG-O) on this aspect, few have addressed the relationship between LIB performance and the degree of reduction of graphene oxide. In this work, we study the performance of LIB anodes using rG-O materials with different oxygen levels. A series of rG-O samples is produced by refluxing an aqueous graphene oxide suspension for different durations. The C/O ratios of the materials are found to increase gradually from approximately 1 to 6, with no heteroatoms other than oxygen atoms. The rG-O sample with the lowest degree of reduction delivers the highest anodic capacity and good durability.

1. Introduction

Li-ion batteries (LIBs) are used in many applications, including portable electronic devices and automobiles, due to their high energy densities and long lifetimes.[1–3] Despite the excellent performances of the graphite-based materials currently used in LIB anodes, graphene-based materials have been suggested as replacements to increase the energy and power densities of the batteries.[4]

Composite materials consisting of graphene-based materials and inorganic nano-particles have shown good performance as anodes in LIB systems.[2,5–7] Among various graphene-based systems, reduced graphene oxide (rG-O) materials, which are produced by the reduction of graphene oxide (G-O), are a prime developmental candidate because of their excellent electrical properties, high surface areas, and feasibility for mass production.[8–10] Although many researchers have investigated rG-O materials in LIB systems, few have addressed the relationship between the performance of the LIB and the reduction degree of G-O. Understanding this relationship is necessary to optimize the performances of graphene-based anodic materials.

G-O contains a large number of oxygen-containing functional groups, such as epoxy and hydroxyl groups on the basal planes and carboxyl and ketone groups at the edges.[11] Although these can be removed by various reduction processes, most rG-O materials retain significant quantities of O atoms.[8–10,12–15] These can affect the chemical and physical properties of rG-O materials.[9,15–18]

Furthermore, many rG-O materials often contain heteroatoms, such as N, P, S, and B, at levels depending on the reduction method used.[8,9,19–22] The presence of such heteroatoms can enhance the performance of the LIB,[22,23] but it also hampers studies the sole role of O atoms in rG-O. Recently, we reported a method allowing fine control of the amount of O in graphene-based materials without contributions from other atomic species.[24] In this study, we prepared a set of refluxed graphene oxide (Re-G-O) materials containing controlled levels of O and studied their performances as LIB anodes.

2. Experimental

2.1 Preparation of a series of Re-G-O and Re-G-O-T samples

Graphite oxide (GO) was synthesized from natural graphite (SP-1, Bay Carbon, USA) using a modified Hummers method.[13] A homogeneous aqueous colloidal suspension of G-O (3 mg mL^{-1} in deionized distilled water) was produced by sonication using a Bransonic 8510 ultrasonic cleaner at 250 W. The suspension was sonicated until it became clear without visible GO particles. The suspension was then immersed in an oil bath and stirred under reflux for different times, as follows: 1 day (Re-G-O-1), 2 days (Re-G-O-2), 3 days (Re-G-O-3), 5 days (Re-G-O-5), or 14 days (Re-G-O-14). The resulting mixtures were filtered with a glass filter; the filtrates were thoroughly washed with water (>10 times) and then dried under vacuum at room temperature for 12 h.

[a]Department of Chemistry and Chemical Engineering, Inha University, Incheon 402-751, Republic of Korea. E-mail: sungjinpark@inha.ac.kr

[b]Faculty of Applied Chemical Engineering, Chonnam National University, Gwang-ju 500-757, Republic of Korea

† Electronic supplementary information (ESI) available: The discharge capacity data; BET surface area and pore information; XPS spectra; MAS SSNMR spectra; FT-IR spectra. See DOI: 10.1039/c5ra13890f

Since battery tests were done with heat-treated Re-G-O samples at 160 °C for 4 h under vacuum, we produced and characterized a second set of samples by heating the above-mentioned samples to produce what we refer to henceforth as Re-G-O-1-T, Re-G-O-2-T, Re-G-O-3-T, Re-G-O-5-T, and Re-G-O-14-T, respectively.

2.2 Electrode fabrication

Electrochemical measurements were performed using a CR2032 coin cell configuration. The electrodes were made by pressing a slurry [72% active Re-G-O material, 14% Ketjen black (KB), and 14% Teflonized acetylene black (TAB)] onto a 200 mm^2 stainless steel current collector and drying both slurry and collector at 160 °C for 4 h in a vacuum oven. The test cells were fabricated in an Ar-filled glove box with Li foil as the cathode, Celgard 3401 as the separator, and 1 M $LiPF_6$ (1 : 1 v/v EC : DMC, Soulbrain Co., Ltd, Korea) as the electrolyte. The charge–discharge characteristics of these cells were evaluated at voltages from 0.01 to 3 V at a range of current densities.

2.3 Instruments and measurements

Elemental analysis was performed with a FLASH EA1112 instrument (Thermo Electron, Italia) under He to determine the C, N, O, and H contents of the samples. X-ray photoelectron spectroscopy (XPS) measurements of the powder samples were performed using an angle-resolved X-ray photoelectron spectrometer (Theta Probe AR-XPS, Thermo Electron Corporation, UK) equipped with a MXR1 Gun-400 μm 15 keV spectrometer. Magic-angle spinning (MAS) solid-state nuclear magnetic resonance (SSNMR) spectra of the powder samples were obtained from 6000 scans on a 600 MHz Varian ^{unity}INOVA (USA), using a HX-MAS probe and a zirconia rotor of 4 mm in diameter. Electrochemical measurements were performed using an electrochemical analyzer (SP-150, Bio-Logic, France). Charge/discharge testing (C-DC) was performed on CR2032 type cells using a BTS 2004 (JAPAN) battery tester at room temperature. Brunauer–Emmett–Teller (BET) surface area measurements (fully automatic physisorption analyzer, Micromeritics, Japan) were performed using N_2 adsorption. Scanning electron microscopy (SEM) images were collected using a field-emission scanning electron microscope (S-4300, Hitachi, Tokyo) at an accelerating voltage of 15 kV. Transmission electron microscopy (TEM) analysis was performed on a field-emission transmission electron microscope (JEM2100F, JEOL, Japan) at 200 kV with samples on a C/Cu grid (HC200-Cu, EMS, USA).

3. Results and discussion

Aqueous homogeneous colloidal suspensions of G-O, produced by the sonication of GO particles in water, were refluxed for designated time periods (1, 2, 3, 5, or 14 days). A set of graphene-based materials (Re-G-O) containing finely controlled amounts of O atoms was produced.[24] Mixtures consisting of the above-mentioned Re-G-O samples and commercial carbon materials were heat-treated at 160 °C for 4 h prior to the examination of their anode performances in LIB cells (Fig. 1).

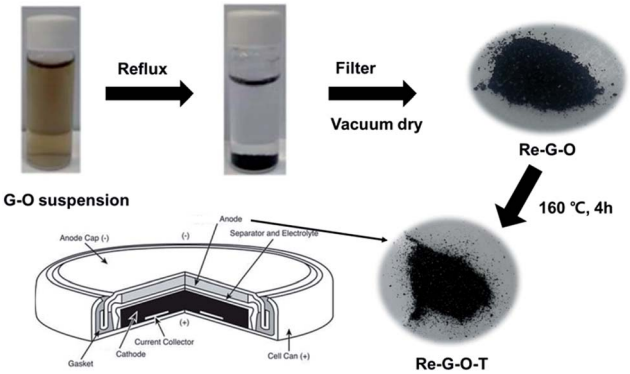

Fig. 1 A scheme for producing Re-G-O and Re-G-O-T samples.

O concentrations in the Re-G-O samples were determined by combustion-based elemental analysis and XPS measurements. The results show that the C/O and C/H ratios of the materials gradually increase as their reflux time increases (Fig. 2a and Table S1†). The lowest O level (C/O ratio of approximately 6) measured in the set of Re-G-O systems is comparable to that of typical rG-O-type materials.[8,9,13,14] Thermal treatment is observed to increase the C/O ratio slightly, and the C/O ratio of

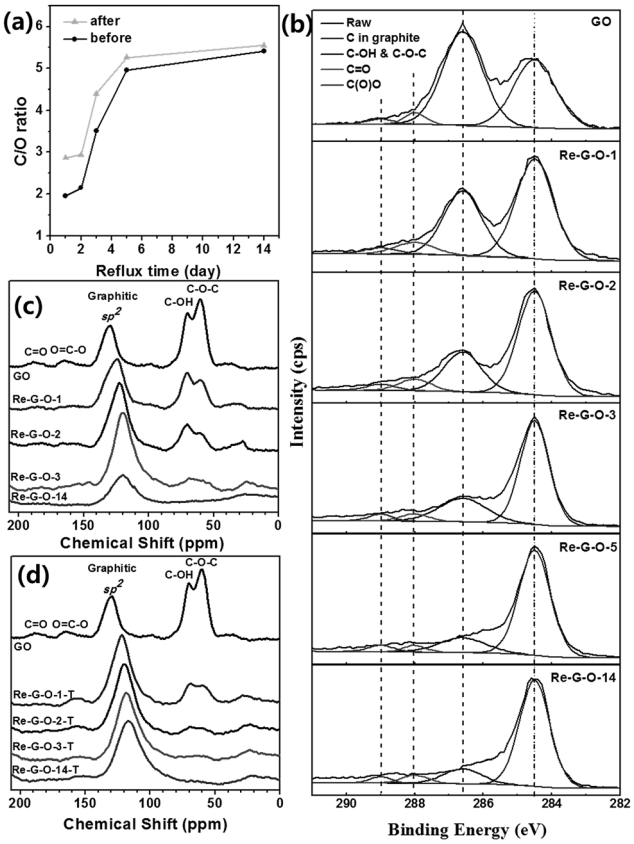

Fig. 2 (a) C/O atomic ratio of Re-G-O (before) and Re-G-O-T (after) samples, measured by combustion-based elemental analysis, (b) deconvoluted XPS C 1s spectra of GO and Re-G-O samples, and MAS SSNMR spectra of (c) GO and Re-G-O samples and (d) Re-G-O-T samples.

the Re-G-O-T samples also gradually increases as their reflux times increase (Fig. 2a).

The XPS C 1s spectrum of GO shows several peaks corresponding to sp^2 carbon, C–O, C═O and C(O)O moieties at 284.5, 286.6, 288.0, and 289.0 eV (Fig. 2b).[25,26] After reflux, the XPS C 1s spectra of the Re-G-O samples show a gradual decrease in the intensity of peaks related to O-based functional groups as the reflux time increases. On comparing the XPS spectra of Re-G-O and Re-G-O-T samples at the same reflux times (Fig. S1, see ESI†), the peak intensity of the O-based functional groups are observed to decrease after the thermal treatment. Since the original G-O was reduced solely by reflux in water, without additional reductants, no heteroatoms other than O are found by either elemental analysis or XPS measurements of the Re-G-O and Re-G-O-T samples.

SSNMR spectroscopy has increasingly been used to probe the chemical structures of graphene-based materials.[27,28] MAS SSNMR spectra of GO, Re-G-O-1, Re-G-O-2, Re-G-O-3, and Re-G-O-14 (Fig. 2c) and of GO, Re-G-O-1-T, Re-G-O-2-T, Re-G-O-3-T, and Re-G-O-14-T (Fig. 2d) show reduction trends consistent with the XPS data. The ^{13}C NMR spectrum of GO shows the presence of O-containing functional groups, including epoxy, hydroxyl, carboxyl, and ketones, and of sp^2 C at 60.3, 70.2, 166.6, 189.0, and 129.4 ppm, respectively.[27,28] As reflux time increases, the intensities of the peaks corresponding to O-containing functional groups decrease (Fig. 2c), reflecting greater degrees of reduction. The peak position of sp^2 C is observed to gradually shift to lower values as the degree of reduction increases. After thermal treatment, the sp^2 C peak shifts slightly further, meaning that the Re-G-O-T samples are slightly more reduced than the Re-G-O samples (Fig. 2d). In addition, the peak intensities of the O-based functional groups are reduced after thermal treatment (Fig. S2†). However, some O-based functional groups still remain. All characterizations show that these series of Re-G-O and Re-G-O-T samples contain finely controlled amounts of O atoms (see ESI† for more characterization), suggesting their suitability for studying the effect of O moieties on their anodic performances in LIBs.

The Re-G-O-T samples were employed as anode materials for LIB applications. Fig. 3 represents the cyclic voltammetry (CV) curves collected within a potential window of 0.01–3 V *vs.* Li at a scan rate of 0.1 mV s^{-1}. During the first cycle, an irreversible peak was observed in the vicinity of ~0.55 V *vs.* Li and becomes unobvious in the subsequent cycles, which is mainly derived from the decomposition of electrolytes.[29–31] The decomposition occurred in an irreversible manner and reductive products forms as a solid electrolyte interphase (SEI) over the active materials consuming more amounts of Li as well. The absence of prominent anodic peaks on the charging process clearly reveals the materials undergo the Li-adsorption/de-sorption reaction rather than the perfect Li-insertion/extraction in graphitic anodes.

The Nyquist impedance spectra were recorded before and after CV measurement for all Re-G-O-T samples as shown in Fig. 4. A typical semicircles observed at high-medium frequency region are associated with the electrolyte resistance (R_s) and the charge-transfer resistance (R_{ct}) across the electrode/electrolyte

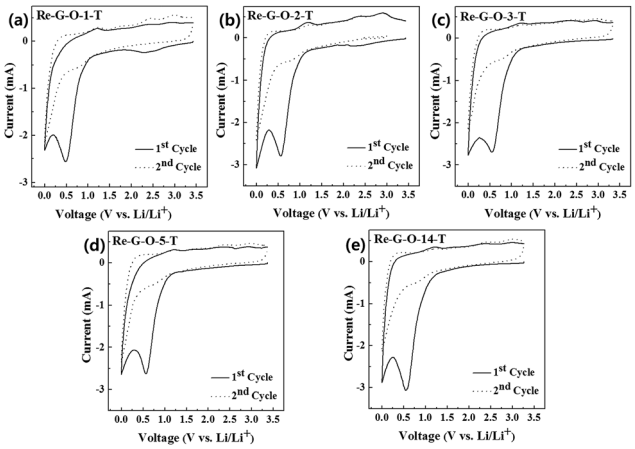

Fig. 3 The CV curve of Re-G-O-T samples at 0.1 mV s^{-1} scan rate; (a) Re-G-O-1-T, (b) Re-G-O-2-T, (c) Re-G-O-3-T, (d) Re-G-O-5-T, (e) Re-G-O-14-T.

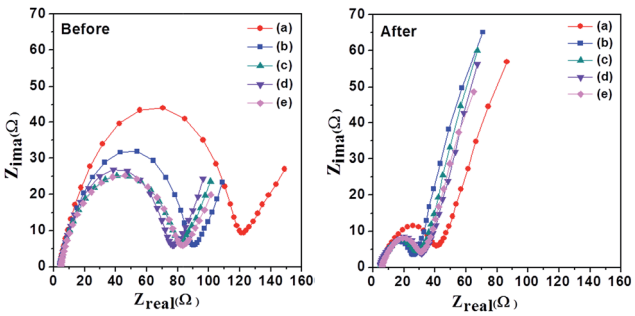

Fig. 4 The Nyquist plots of all Re-G-O-T samples recorded at before and after CV measurements: (a) Re-G-O-1-T, (b) Re-G-O-2-T, (c) Re-G-O-3-T, (d) Re-G-O-5-T, (e) Re-G-O-14-T.

interfaces.[32,33] The R_{ct} value for Re-G-O-1-T and Re-G-O-14-T are 122 and 84 Ω before cycling, respectively. After CV measurement, the R_{ct} values for Re-G-O-1-T and Re-G-O-14-T decreased dramatically from 122 to 43 Ω and 84 to 32 Ω, respectively, which may be related to the stabilization of SEI layer.[34–37]

Galvanostatic charge–discharge cycles were carried out up to 60 cycles between 0.01–3.0 V *vs.* Li at the constant current

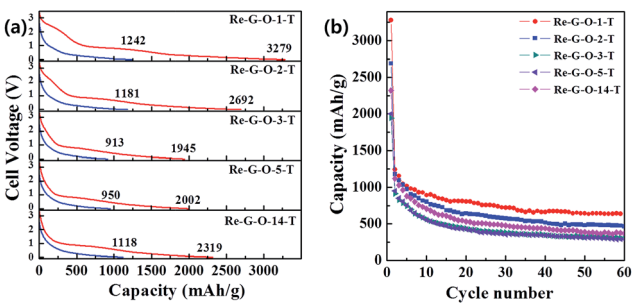

Fig. 5 (a) Comparison 1st and 2nd discharge curves for Re-G-O-T samples, (b) cycling performance at 100 mA g^{-1}.

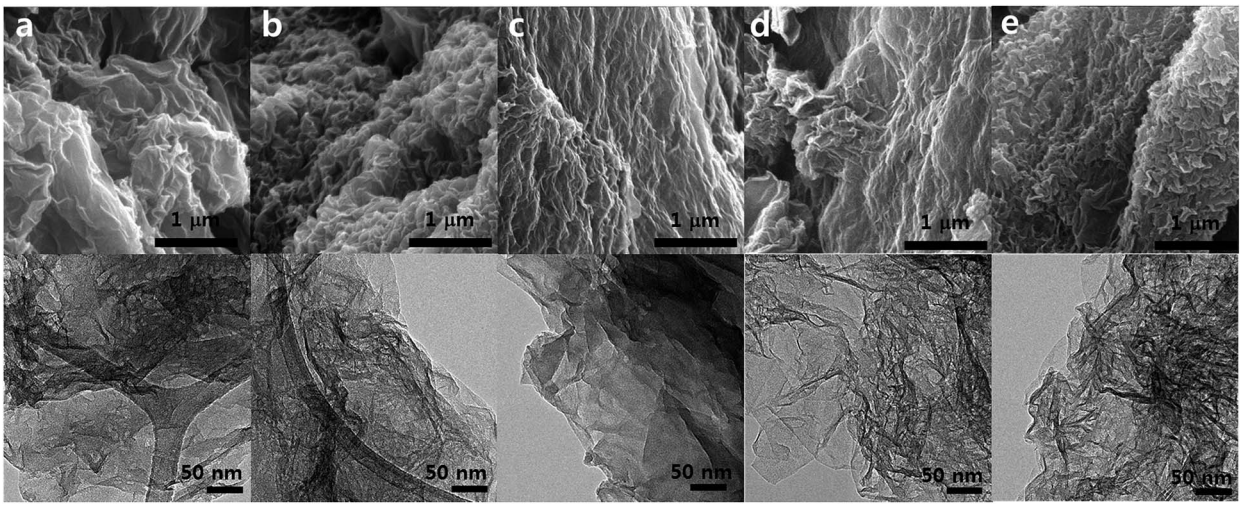

Fig. 6 SEM and TEM images of (a) Re-G-O-1-T, (b) Re-G-O-2-T, (c) Re-G-O-3-T, (d) Re-G-O-5-T, and (e) Re-G-O-14-T.

density of 100 mA g^{-1} and given in Fig. 5. Fig. 5a shows the typical discharge curves of Re-G-O-T samples. The discharge capacity of Re-G-O-1-T is found to be ~3279 and ~1242 mA h g^{-1} for first and second cycles, respectively. A huge irreversible capacity loss of ~62% is observed. This loss could be mainly due to the decomposition of the electrolyte solution and subsequent SEI formation. The first discharge curve for all Re-G-O-T samples exhibits the plateau at ~1.3 and ~0.6 V *vs.* Li and it is consistent with the onset potential of observed from the CV studies. As expected, the 2nd cycle showed no plateaus, because decomposition of electrolytes occurred in an irreversible manner. Discharge capacities of all Re-G-O-T samples at the 1st, 2nd and 50th cycles were compared in Table S2.† The cycling performances of all Re-G-O-T are shown in Fig. 5b. The discharge capacity of Re-G-O-1-T (up to 55% in the 60th cycle) is much higher than other Re-G-O-T samples. The discharge capacity is still remains ~637 mA h g^{-1} after the 60th cycle, corresponding to ~51% of the second discharge capacity. The degree of refluxing time increases; the discharge capacity is decreasing and reaching minima in Re-G-O-14-T (~370 mA h g^{-1} at the 60th cycle, which has the highest degree of reduction). The above results can be ascribed to that O-containing moiety improve the Li^+ intake ability on prolonged cycling.

The morphological features of the Re-G-O-T samples were investigated by SEM and TEM. All images show agglomerations of exfoliated thin graphene-based materials; morphologies are maintained regardless of the degree of reduction (Fig. 6). BET measurements of each material's specific surface area (SSA) and pore information are shown in Table S3.† Interestingly, the Re-G-O samples showing high Li^+ capacity values (Re-G-O-1 and Re-G-O-14) have about 50% smaller SSA values than other samples (Re-G-O-3 and Re-G-O-5). However, these surface area values remain significantly larger than (about two order) those of typical graphite-based electrode materials.[38–40] The average pore diameter of the Re-G-O-1 sample is much larger than those of other samples (Table S3†). Since graphene-based systems fabricated by solution processing typically have agglomerated morphologies, their pore sizes may be an important factor for the movement of Li^+. Furthermore, theoretical calculation suggested that Li^+ diffusion can be enhanced along perpendicular direction to the graphene-based layers when graphene-based electrodes have double vacancy and higher-order defects.[41] Consequently, many defect sites and large pores with high surface areas could be one of the reasons for high capacity values of the Re-G-O-1 sample.

4. Conclusions

We studied the LIB anode performances of rG-O materials with different O levels (C/O ratios from 1 to 6). A series of Re-G-O materials was produced by refluxing aqueous G-O suspensions for different times. The chemical and morphological characterizations of these materials were performed by NMR, XPS, BET, SEM, and TEM, confirming the fine control of O levels. Re-G-O-1 sample, which features the lowest degree of reduction, delivers high capacity and improves durability relative to the other samples. This finding will aid in optimizing the LIB performances of graphene-based anode materials derived from G-O.

Acknowledgements

S. P. thanks the Busan Center at the Korean Basic Science Institute (KBSI) for the XPS analysis. This work was supported by grants from INHA University, and a grant from the International Cooperation of the Korean Institute of Energy Technology Evaluation and Planning (KETEP) funded by the Korean Ministry of Knowledge Economy (Grant no. 20128510010050).

References

1 J. Tarascon and M. Armand, *Nature*, 2001, **414**, 359–367.
2 P. G. Bruce, B. Scrosati and J. Tarascon, *Angew. Chem., Int. Ed.*, 2008, **47**, 2930–2946.

3 J. B. Goodenough and Y. Kim, *Chem. Mater.*, 2009, **22**, 587–603.
4 J. Hou, Y. Shao, M. W. Ellis, R. B. Moore and B. Yi, *Phys. Chem. Chem. Phys.*, 2011, **13**, 15384–15402.
5 D. Xue, S. Xin, Y. Yan, K. Jiang, Y. Yin, Y. Guo and L. Wan, *J. Am. Chem. Soc.*, 2012, **134**, 2512–2515.
6 Y. Sun, X. Hu, W. Luo and Y. Huang, *ACS Nano*, 2011, **5**, 7100–7107.
7 G. Zhou, D. Wang, P. Hou, W. Li, N. Li, C. Liu, F. Li and H. Cheng, *J. Mater. Chem.*, 2012, **22**, 17942–17946.
8 S. Stankovich, D. A. Dikin, R. D. Piner, K. A. Kohlhaas, A. Kleinhammes, Y. Jia, Y. Wu, S. T. Nguyen and R. S. Ruoff, *Carbon*, 2007, **45**, 1558–1565.
9 J. Han, L. L. Zhang, S. Lee, J. Oh, K. Lee, J. R. Potts, J. Ji, X. Zhao, R. S. Ruoff and S. Park, *ACS Nano*, 2013, **7**, 19–26.
10 S. Pei and H. Cheng, *Carbon*, 2012, **50**, 3210–3228.
11 H. He, J. Klinowski, M. Forster and A. Lerf, *Chem. Phys. Lett.*, 1998, **287**, 53–56.
12 S. Lee and S. Park, *Carbon Lett.*, 2012, **13**, 48–50.
13 S. Park, J. An, R. D. Piner, I. Jung, D. Yang, A. Velamakanni, S. T. Nguyen and R. S. Ruoff, *Chem. Mater.*, 2008, **20**, 6592–6594.
14 H. Shin, K. K. Kim, A. Benayad, S. Yoon, H. K. Park, I. Jung, M. H. Jin, H. Jeong, J. M. Kim and J. Choi, *Adv. Funct. Mater.*, 2009, **19**, 1987–1992.
15 H. Guo, X. Wang, Q. Qian, F. Wang and X. Xia, *ACS Nano*, 2009, **3**, 2653–2659.
16 B. Zhao, P. Liu, Y. Jiang, D. Pan, H. Tao, J. Song, T. Fang and W. Xu, *J. Power Sources*, 2012, **198**, 423–427.
17 F. Liu and D. Xue, *Chem.–Eur. J.*, 2013, **19**, 10716–10722.
18 J. Yan, L. Xian and M. Chou, *Phys. Rev. Lett.*, 2009, **103**, 086802.
19 S. Lee, J. R. Potts, J. Oh, J. Han, G. Park and S. Park, *Solid State Sci.*, 2014, **27**, 1–4.
20 U. N. Maiti, W. J. Lee, J. M. Lee, Y. Oh, J. Y. Kim, J. E. Kim, J. Shim, T. H. Han and S. O. Kim, *Adv. Mater.*, 2014, **26**, 40–67.
21 Z. Yang, Z. Yao, G. Li, G. Fang, H. Nie, Z. Liu, X. Zhou, X. Chen and S. Huang, *ACS Nano*, 2011, **6**, 205–211.
22 C. Zhang, N. Mahmood, H. Yin, F. Liu and Y. Hou, *Adv. Mater.*, 2013, **25**, 4932–4937.
23 Z. Wu, W. Ren, L. Xu, F. Li and H. Cheng, *ACS Nano*, 2011, **5**, 5463–5471.
24 G. Park, S. K. Park, J. Han, T. Y. Ko, S. Lee, J. Oh, S. Ryu, H. S. Park and S. Park, *RSC Adv.*, 2014, **4**, 36377–36384.
25 S. Park, K. Lee, G. Bozoklu, W. Cai, S. T. Nguyen and R. S. Ruoff, *ACS Nano*, 2008, **2**, 572–578.
26 D. Yang, A. Velamakanni, G. Bozoklu, S. Park, M. Stoller, R. D. Piner, S. Stankovich, I. Jung, D. A. Field and C. A. Ventrice, *Carbon*, 2009, **47**, 145–152.
27 W. Gao, L. B. Alemany, L. Ci and P. M. Ajayan, *Nat. Chem.*, 2009, **1**, 403–408.
28 W. Cai, R. D. Piner, F. J. Stadermann, S. Park, M. A. Shaibat, Y. Ishii, D. Yang, A. Velamakanni, S. J. An, M. Stoller, J. An, D. Chen and R. S. Ruoff, *Science*, 2008, **321**, 1815–1817.
29 C. Wang, D. Li, C. O. Too and G. G. Wallace, *Chem. Mater.*, 2009, **21**, 2604–2606.
30 L. David and G. Singh, *J. Phys. Chem. C*, 2014, **118**, 28401–28408.
31 G. Wang, X. Shen, J. Yao and J. Park, *Carbon*, 2009, **47**, 2049–2053.
32 J. Vetter, P. Novák, M. Wagner, C. Veit, K. Möller, J. Besenhard, M. Winter, M. Wohlfahrt-Mehrens, C. Vogler and A. Hammouche, *J. Power Sources*, 2005, **147**, 269–281.
33 X. Jia, Z. Chen, X. Cui, Y. Peng, X. Wang, G. Wang, F. Wei and Y. Lu, *ACS Nano*, 2012, **6**, 9911–9919.
34 P. Lian, X. Zhu, S. Liang, Z. Li, W. Yang and H. Wang, *Electrochim. Acta*, 2010, **55**, 3909–3914.
35 P. Guo, H. Song and X. Chen, *Electrochem. Commun.*, 2009, **11**, 1320–1324.
36 Z. Jiang and Z. Jiang, *ACS Appl. Mater. Interfaces*, 2014, **6**, 19082–19091.
37 M. Yazici, D. Krassowski and J. Prakash, *J. Power Sources*, 2005, **141**, 171–176.
38 M. K. Datta and P. N. Kumta, *J. Power Sources*, 2007, **165**, 368–378.
39 N. Dimov, S. Kugino and M. Yoshio, *J. Power Sources*, 2004, **136**, 108–114.
40 M. Wagner, P. Raimann, A. Trifonova, K. Moeller, J. Besenhard and M. Winter, *Electrochem. Solid-State Lett.*, 2004, **7**, A201–A205.
41 X. Fan, W. Zheng and J. Kuo, *ACS Appl. Mater. Interfaces*, 2012, **4**, 2432–2438.